Towards a Measurement of the $W + 2\ jets$ and $Wb\bar{b}$ Production Cross Section at $\sqrt{s} = 1.96$ TeV

Stéphanie Beauceron, Gregorio Bernardi and Sophie Trincaz-Duvoid

LPNHE, Universités Paris VI and VII,
IN2P3-CNRS, Paris, France

DRAFT 1.0, 07/27/2003

Abstract

The first steps towards a measurement of the $W + 2\ jets$ and $Wb\bar{b}$ production cross section at $\sqrt{s} = 1.96$ TeV in the $e+\not{E}_T$ final state are presented.

Contents

1 Introduction

The $Wb\bar{b}$ channel plays a special role at the Tevatron since it is an important background for Higgs and single top production. The measurement of its cross-section will allow to test our understanding of the higher order production of the W's. This channel also provides a clean benchmark of the capabilities of the detector concerning b-jets, missing E_T ($\not\!\!E_T$) and lepton identification/calibration.

Our measurement is based on the $W+\ 2jets$ channel producing the $e+\not\!\!E_T$ final state, to which different types of b-tagging are applied. The properties of $W+\ n$ jets events are presented and compared to simulation expectations.

2 Data Sample

The data used for this analysis has been reconstructed with the versions p13.05.00 and p13.06.01 of the DØ reconstruction software, taken between August 15^{th} 2002 and June 24^{th} 2003, amounting to a luminosity, after data selection, of 117.4 pb^{-1}.

The W candidates have been selected using the inclusive single electron skim provided by the WZ working group. This skim selects all events with at least one reconstructed electron candidate (ID=10,11) with $p_T > 15$ GeV. Additionally only events passing a trigger requesting at least one EM object and having a low downscale are used.

The following corrections have also been applied to our dataset:

- "shared energy problem" due to bad BLS [1];
- correction to the bug in the n90/f90 jet variable (as implemented in p14-br-03);
- new jet seeding (as implemented in DØReco p14.01) which slightly reduce the influence of fake jets.

The corrections are applied when we pass the skimmed WZ sample through the TopAnalyze package [2] which creates the analysis root-tuples.

To ensure that only data of reasonable quality are used, only events which are not rejected as bad runs by the JETMET group have been selected [3]. The runs flagged "bad" by the CAL [4],SMT [6] and CFT [5] groups are also rejected. The resulting luminosity used (117.4 pb^{-1}) is about 21% smaller than the total recorded luminosity during the period under consideration.

3 Luminosity and Trigger

The luminosity corresponding to the data sample is calculated following the Luminosity-ID group instructions [7]. For determining the luminosity a list of all luminosity block numbers (LBN) is built from the complete raw data on which the data sample is based. The luminosity is then summed up by the LM-access tool [7] which gives the luminosity of the reconstructed events for a given trigger.

The list of triggers available, and the fraction of luminosity, weighted by their downscale fraction are given in table 1. An 'OR' of the triggers given in this table (excepting the last 7 ones which cover only a low equivalent luminosity during this period) is used for the cross-section measurement. The trigger efficiency is obtained on the full dataset using muon-based triggers. The "turn on" curve obtained is shown in figure 1a). In figure 1b) is shown the fitted curve used to weight the simulation. The uncertainty on the measured luminosity is assumed to be 10%.

4 Simulated Data Sets

The following processes, which are used to compare with the data: have been simulated with the Pythia [10] MC event generator version 6.202, making use ofthe CTEQ5L [12] parton distribution functions.

- inclusive $W \to e\nu$ production (96241 events / 3054 pb)
- inclusive $Z \to ee$ production (25500 events / 294 pb)
- inclusive $W \to \tau\nu$ production (49750 events / 3054 pb)
- inclusive $Z \to \tau\tau$ production (24750 events / 294 pb)
- $t\bar{t} \to e$ + jets production (11000 events / 0.9 pb / m_{top}= 175 GeV)
- exclusive $WH \to e\nu b\bar{b}$ production (49000 events / 0.02 pb / m_H= 115 GeV)
- exclusive $Wb\bar{b}$ production (23341 events / 4.0 pb) is generated with the ALPGEN generator [11] since it has a better simulation of high jet multiplicity processes. To avoid double counting, $Wb\bar{b}$ events produced by Pythia in the inclusive sample are explicitely removed.

These events have been processed through the DØ detector simulation (DØgstar [13], based on GEANT), the electronics simulation (DØsim) and the reconstruction software (DØreco). The simulated events are then reweighted by the trigger efficiency and by the ratio between data and simulation for the track efficiency (0.92 $\pm$0.03) and for the electron reconstruction efficency (0.88 $\pm$0.03 [8]). The normalization of the overall simulated background (which are normalized among themselves according to cross-section) is allowed to move within the uncertainty of the luminosity measurement (10%) such that the total number of electrons of the simulation match the number of electrons in the final sample. The normalization factor required is 1.01, well inside the systematic error of the DØ luminosity measurement, and lower than the typical error on the production cross-section of the background processes ($> 5\%$). This shows that we are consistent with the DØ W cross-section measurement obtained for the 2003 winter conferences.

Trigger	Mean live fraction (when present)	Mean live fraction (averaged over full data set)	Luminosity (averaged over full data set)
EM_MX	1.000	1.000	117.411
2EM_HI	0.989	0.989	116.094
EM_MX_EMFR8	1.000	0.987	115.929
EM_MX_SH	1.000	0.987	115.929
EM_MX_TR	1.000	0.987	115.929
EM15_2JT15	0.989	0.966	113.469
EM_HI_SH	0.930	0.929	109.065
EM_HI_EMFR8	0.930	0.929	109.065
EM_HI	0.930	0.929	109.065
EM_HI_SH_TR	0.930	0.929	109.065
EM_HI_TR	0.930	0.929	109.065
EM_MX_SH_TR	1.000	0.916	107.521
EM_HI_2EM5_TR	0.935	0.895	105.143
EM_HI_2EM5_SH	0.935	0.895	105.143
EM_HI_2EM5_SH_TR	0.935	0.895	105.143
EM_HI_2EM5	0.935	0.895	105.143
2EM_HI_EMFR8	1.000	0.803	94.257
EM_MX_F0	1.000	0.803	94.257
2EM_HI_SH	1.000	0.803	94.257
2EM_HI_SH_TR	1.000	0.803	94.257
EM15_2JT25	1.000	0.803	94.249
EM_HI_F0	0.991	0.794	93.233
2EM_2MD12	0.989	0.770	90.426
EM_HI_METSH	1.000	0.747	87.761
EM_HI_METF0	1.000	0.747	87.761
EM_HI_2EM5_F0	0.983	0.747	87.748
EM_HI_2EM5_METSH	0.984	0.706	82.877
EM_HI_2EM5_METF0	0.984	0.706	82.877
2EM_2MD7	0.637	0.584	68.596
EM_MD_2CJT5	0.017	0.017	1.957
EM_LO	0.005	0.005	0.550
EM_LO_SH	0.005	0.005	0.550
EM_HI_SH12	0.006	0.004	0.462
CEM10_2CJT5	0.004	0.003	0.359
CEM5	0.000	0.000	0.007

Table 1: An 'OR' of the triggers given in this table (excepting the last 7 ones which have low luminosity) is used for the cross-section measurement. The resulting efficiency is obtained on the full dataset using muon-based triggers. The difference between the luminosity number given here and the overall slight lower luminosity used in the analysis is due to a small subset of the data (~ 1.2 pb^{-1}) which has not been processed yet.

5 Event Selection

The analysis is based on the selection of events with at least one electron with $p_T > 20$ GeV and missing transverse momentum $\not{E}_T > 25$ GeV. The electron is required to have $\eta_{detector}$ within ± 1.1 and to be oustide the standard DØ φ module boundaries [8]. These general criteria define our final data sample. We detail in the following the electron identification, the QCD background rejection and the missing E_T requirement.

5.1 Electron identification

The identification of electrons for this analysis follows the recommendations of the EM-ID group [8]. Electrons are identified mainly by their characteristic energy deposition in the calorimeter of the detector. Possible candidates for electrons are determined by searching for energy depositions larger than a certain threshold within a cone of radius $R < 0.2$ in the $(\eta, \varphi))$ plane. These electron candidates are then required:

- to have a large energy fraction : $EMF > 0.9$. The distribution of the EM fraction for the electrons of the final sample is shown in figure 2a.
- to be isolated: the energy outside the 0.2 electron cone and inside a cone of 0.4, normalized to the 0.2 cone energy must be lower than 0.15. The distribution of the isolation for the electrons of the final sample is shown in figure 2b.
- the cluster of the candidate must be electromagnetic like, and this is enforced using a cut on the standard DØ H-Matrix (8 parameters) [8] at 20. The distribution of the H-Matrix χ^2 for the electrons of the final sample is shown in figure 2c. It is not well modelled in the simulation and this discrepancy is taken into account in the systematic error of the electron identification.
- to have a track pointing to the EM cluster. EM clusters w/o tracks are called loose electrons and are used to estimate the background since this sample is populated by electrons in which the track reconstruction was inefficient, and by jets in which appear an isolated EM cluster. The multiplicity of electrons in the final sample is shown in figure 2d.

The inefficiency induced by these requirements is dominated by the cut on the H-Matrix and by the track inefficiency. In the following we determine separately the id-efficiency (first 3 requirements), from the track efficiency.

Both efficiencies are determined from our final sample in which we removed the $\not{E}_T$ cut: we thus can select a complete sample of Z events. On the Z events, defined here as 2 electrons with $p_T > 20$ GeV, the id-efficiency is determined by comparing the number of events in which one of the electron fails the 3 id cuts (but is still track matched), to the total number of Z events. The id-reconstruction efficiency is found to be $87.9\% \pm 3\%$ (stat.+syst.) in agreement with the benchmark numbers provided by the EM-id group $(85.0\% \pm 2\%)$.

The track-matching efficiency is determined using the samples of N_2 events with 2 electrons and the sample of N_1 one electron+one loose electron (i.e. no track-match). The track-matching efficiency ϵ is then given by:

$$\epsilon = \frac{2 \cdot N_2}{N_1 + 2 \cdot N_2}$$

The numbers N_1 and N_2 of Z events are calculated in the di-electron invariant mass window between 80 GeV and 100 GeV. The track match efficiency for electrons in the central region is thus determined to be $75.8\% \pm 3\%$.

The distributions for the $Z \to ee$ events which have been used to determine the track efficiency are shown in figure 3. These distributions are shown after adjustment of the energy response of the simulated electrons: a rescaling of the energy of -1.5% and an additional smearing of 4% have been added to have a better description of the data by the simulation.

5.2 QCD fake rate and QCD background

For estimating the number of QCD events passing the electron identification we need to know the probability for a fake electron to have a track match. For this calculation a data sample is built from a dijet sample back to back in φ ($|\Delta\varphi| < 0.002$), at low $\not{E}_T (< 10$ GeV), and in which one of the jets has an EM fraction smaller than 0.7, in order to reject Z events, and the other pass all the electron-id requirements except the track match. The fake rate probability is obtained by dividing the number of events in which the electron candidate has no track matching by the number in which the electron candidate has a track matching, and we obtain $2.4\% \pm 0.2\%$ in agreement with previous determinations obtained on a smaller dataset [14].

The QCD background is then estimated for every differential distribution using the matrix method [14] applied to our final sample and to the loose sample (defined with the same cuts as the final sample but requesting one candidate electron with or w/o track matching, instead of an electron). The effect of the track-matching request, and the variation of the QCD background is shown as an example on the p_T distribution of the electron candidate, in figure 4 for the loose and final sample respectively.

The distributions of the energy, p_T, η and φ of the electrons of the final sample are shown in figure 5.

5.3 Missing E_T Requirement and W Transverse Mass

Since we want to select W's decaying in the electron mode, we place a cut on the transverse missing energy:

$$\not{E}_T \ > 25\text{Gev}$$

The calorimetric Missing E_T is calculated according to the JETMET prescription (remove unclustered energy in the CH calorimeter for the $\not{E}_T$ calculation). $\not{E}_T$ is also corrected for muons. All corrections to the electrons or to the jets are propagated in the $\not{E}_T$ calculation. The systematic associated to the $\not{E}_T$ cut is obtained by varying the Jet energy scale and the electron within their systematics error ($\pm 6\%$ and $\pm 2\%$) respectively.

The distributions of $\not{E}_T$ of the azimuthal angle of the $\not{E}_T$ vector, and of the x and y components of $\not{E}_T$ are shown for the final sample in figure 6.

The transverse mass and the p_T of the W can be reconstructed from the electron and missing energy kinematics. The results of their reconstruction are shown in figure 7a,b respectively. A good agreement is observed between the measured and simulated data. Note that similar distributions produced for the W cross section measurement have been obtained using a fast simulation (PMCS), while in this analysis all processes have been produced with a detailed simulation (plate geometry).

6 Jet Properties

The jets used in this analysis are Run II cone type jets with a radius of R = 0.5 identified following the recommendations of the JETMET group [3]. The jets multiplicities and properties are distorted by the presence of so-called fake jets which is reduced by the jet-id criteria. Fake jets are either created by fake energy in the calorimeter (electronics misfunction in some region of the calorimeter), or are real low energy jets which collect sufficient fake energy to pass the energy thresholds cuts. Since distinguishing between these two cases on an event by event basis is not straightforward, the JETMET group has developed a set of ID cuts which allow to classify the jets as "good" or "bad". The jets are not actually rejected, but the energy of the "bad" jets are not corrected and this diminishes their influence on the event kinematics. In the following "jets" will always refer to "good jets".

The following two cuts ensure that the jet energy distribution in the various layers of the calorimeter is reasonable:

- the energy fraction in the electromagnetic layers of the jet is required to be $0.05 < EMF < 0.95$.
- The energy fraction in the outermost layer (coarse hadronic) is required to be $CHF < 0.4$.
- Since jets are relatively broad objects it is expected that the energy is found in several calorimeter towers which have a size of $0.1 \cdot 0.1$ in the (η, φ) plane, hence the number of towers containing 90% of the jet energy ($n90$)is required to be larger than 1 ($n90 > 1$).
- Another source of fake jets are due to "hot" cells. To remove this type of fake jet it is required that the ratio of the energy in the hottest cell to the next-hottest is not too large: HOTF < 10.
- Finally, to remove a special type of fake jets which are due to a high CH noise a new quantity has been introduced: $f90 = n90/nitm$ ($nitm$ = total number of towers). This quantity has recently been found to be wrongly calculated in DØReco [3], for jets which underwent a merging of two (or more) lower energy jets. The jet code has been fixed [3] and we reprocessed the skimmed events with the new code. We are thus using the new criteria provided by the JETMET group: a good jet is also required to have $f90 < 0.5$ or $CHF < 0.15$.

The distributions of the main estimators (EMF, CHF, f90) and p_T are shown in figure 8a,b,c,d respectively. The normalization of the plots regarding jets are relative (the total number of MC jets is normalized to the total number of jets of the data after subtraction of the QCD background). The normalization factor (Data-QCD/MC) for the jets is found to be 1.21 and can be attributed to the lower jet multiplicity generated by Pythia, but can also be influenced by the jet energy scale: if the jet energy scale correction of the data is overestimated, the number of jets passing the threshold is higher. When varying the jet energy scale on the simulated events by its uncertainty ($\pm 6\%$ in average) [9] , the number of simulated jets increases by a factor of $+16/-22\%$. We can thus attribute, on top of the systematics due to the Jet energy scale uncertainty an additional systematics on the jets multiplicity of 14% (from the quadratic difference of 21% and 16%)

The distributions of the jet multiplicity and p_T (in linear and log scale are shown in figure 9. The distributions of the p_T of the first 4 jets are shown in figure 10. The shapes and slopes are described over the complete kinematic range. However the expectation distribution for the second jet displays a departure from the measured slope which can be attributed, at least in part, to a deficit of hard high multiplicity jet in Pythia. The same distributions are shown in figure 11 after having applied a positive shift on the simulated jet energies of the size of the jet energy scale uncertainty. The agreement becomes better, hinting that the data might be slightly overcalibrated.

7 Dijet mass and b-tagging Results

The distribution of the invariant mass of the 2 leading jets, in events where there are at least two jets is shown in figure 13a and b. The shape of the distribution is well described by the simulation. The number of simulated dijet events is underestimated due to the lower number of 2/3 jets events in the simulation.

In figure 13c,d we plot the dijet mass distributions in which one jet has been tagged as b-jets by the JLIP algorithm[15], which is based on the estimation of the probability to observe the b lifetime. We cut as prescribed by the JLIP authors on a jet lifetime probability smaller than 1%, which has been studied to create a tagging of light quarks (fake rate) of $1.1 \pm 0.1\%$. For this fake rate, the tagging efficiency is expected to be $35 \pm 2\%$ (the taggability is expected to be around 70% in a single jet QCD sample). For the distributions related to b-jet tagging, the ratio between the expected tagging $\times$ taggability efficiency in data and simulation (0.85×0.82) has been used to reweight the simulation. The observed number of single tagged events in the data are 92 events. Once the QCD background (12 events) has been subtracted, we observe 80 single b-tag events to be compared to 78.1 expected events, The breakdown of the different contributions are given in the boxes associated to figures 13c and d. Here we can notice a good description of the data by the Standard Model backgrounds, both in shape and in amplitude.

In figure 14a,b,c,d are shown the distributions for the H_T variable, which is defined as the sum of the E_T of the jets in the event, for the untagged events, and for the events which have one JLIP b-tagging. The same conclusions as for the dijet mass can be drawn from these plots.

In figure 15a,b,c,d are shown the distributions for the ΔR variable (distance in the $\eta - \varphi$ plane between the two leading jets), for the untagged events, and for the events which have one JLIP b-tagging. Here again, a good description of the b-tagged data, both in shape and in amplitude, is made by the simulation.

Since the single b-tag jets distributions are well described, we study the events having at least 2 jets being b-tagged. In figure 16 are shown the distributions for the p_T of the b-tagged jets: in a),c) for the sample having only one jet being b-tagged, in b),d) for the sample in which at least 2 jets have been b-tagged. A good agreement is observed in both cases. In the case of double b tags, 3 events survive our selection, for an expected standard model prediction of 3.3 events.

In figure 17a,b,c are shown the invariant mass, H_T and ΔR distributions for the events having at least 2 jets being b-tagged. In figure 17d is shown the multiplicity distribution of the b tagged jets in the complete sample.

8 Summary

The inclusive $W \to e\nu$ has been studied on 117.4 pb of data taken between the 15^{th} of August 2002 and 24^{th} June 2003, processed with the p13.05 and p13.06 reconstruction version. The data are well described by the simulated Standard Model processes for the inclusive production rate, while the jet production rate in these events tend to be higher than the production rate obtained in the simulation. The number of events with at least 2 jets are present, with at least one (two) jets has been tagged as a b jet has been studied, using the JLIP algorithm, and compared to the expectation from simulation. The production rate is in agreement with the expectation from Standard Model processes, within statistical and systematic errors.

Acknowledgments

We would like to thank the Higgs, Top and WZ groups and all the ID groups related to this note (EM, JETMET, JES, b-id, Luminosity) for the input they have provided to obtain the results presented in this analysis. We also would like to thank in particular Emmanuel Busato, Marumi Kado, Markus Klute Marco Verzocchi, Jean-Roch Vlimant and Robert Zitoun for their great help. Thanks also to Avto Kharchilava and John Hobbs for their advice and help during the completion of this work.

References

[1] http://www-d0.fnal.gov/ d0upgrad/calelec/caltf/Welcome.html

[2] http://www-clued0.fnal.gov/ klute/general/TopAnalyze.html

[3] JETMET group, Certification Results 3.1 and 3.2, http://www-d0.fnal.gov/ d0upgrad/d0_private/software/jetid/jetid.html

[4] DØ Calorimeter Technical Design Report, http://www-d0.fnal.gov/ d0upgrad/calelec/intro/tdr/tdrformat.htm

[5] DØ Central Fiber Tracker, http://d0server1.fnal.gov/projects/SciFi/cft_description.html http://d0server1.fnal.gov/users/stefan/www/CFT_TDR/CFT_TDR.d

[6] DØ Silicon Tracker Technical Design Report, http://d0server1.fnal.gov/projects/silicon/www/tdr_final.ps

[7] Luminosity ID group: http://www-d0.fnal.gov/phys_id/luminosity/data_access/

[8] EM-ID group, Certification Results Version 2.0, http://www-d0.fnal.gov/phys_id/emid/d0_private/certification/main_v2_0.html

[9] Jet Energy Scale group http://www-d0.fnal.gov/phys_id/jes/d0_private/latest/v4.1/links.html

[10] T. Sjostrand, P. Eden, C. Friberg, L. Lonnblad, G. Miu, S. Mrenna and E. Norrbin, "High-energy-physics event generation with PYTHIA," Comput. Phys. Commun. **135**, (2001) 238

[11] M. Mangano et al.: ALPGEN, a generator for hard multiparton processes in hadron collisionsJ, hep-ph/0206293

[12] H. L. Lai et al., "Improved Parton Distributions from Global Analysis of Recent Deep Inelastic Scattering and Inclusive Jet Data", Phys.Rev. D55 (1997) 1280

[13] Y. Fisyak and J. Wormesley, DØ-Note 3191

[14] M. Kado and R. Zitoun, DØ Note 4004

[15] D. Bloch et al., DØ Note 4069,4158,4159

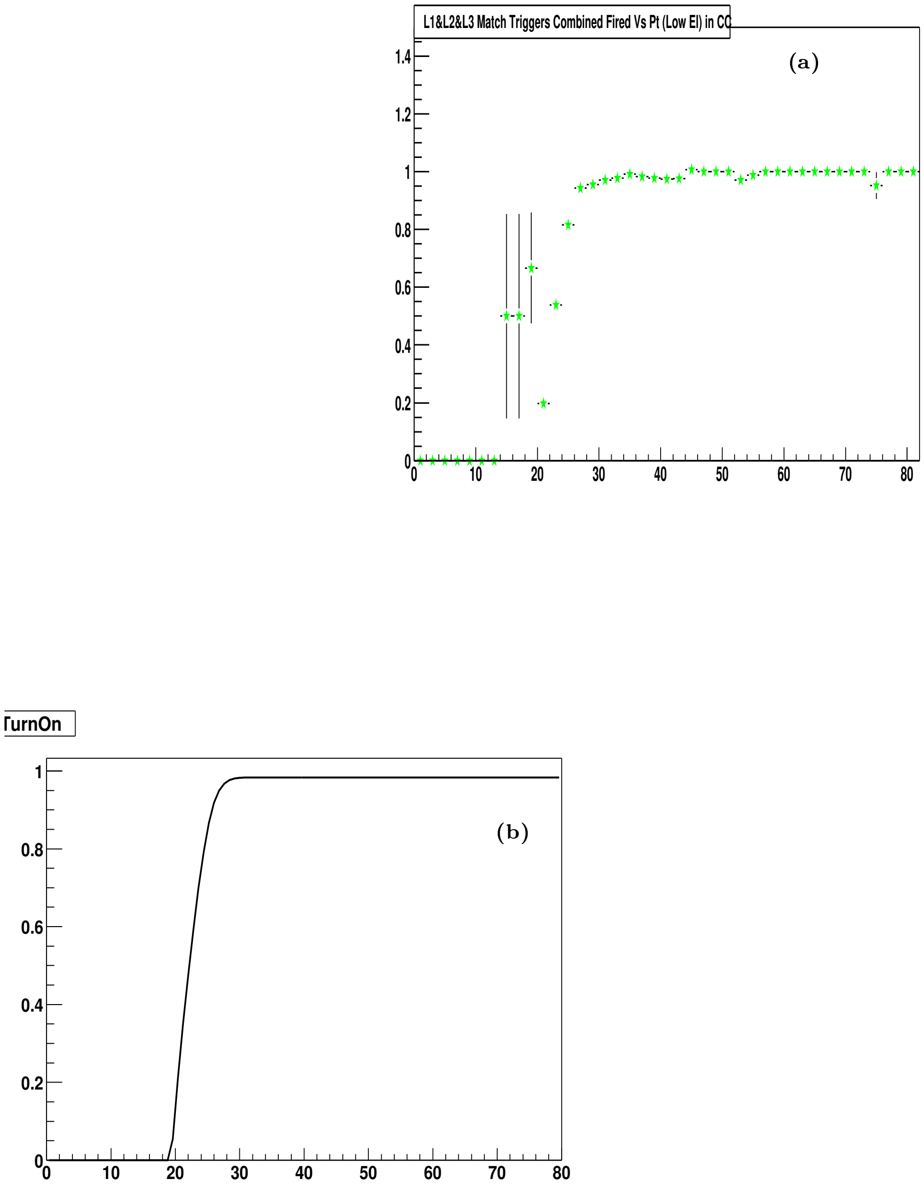

Figure 1: a) Trigger turn-on curve for the trigger mix used, obtained from the full data sample using muon triggers as reference. b) fitted curve to the points, used to weight the simulation.

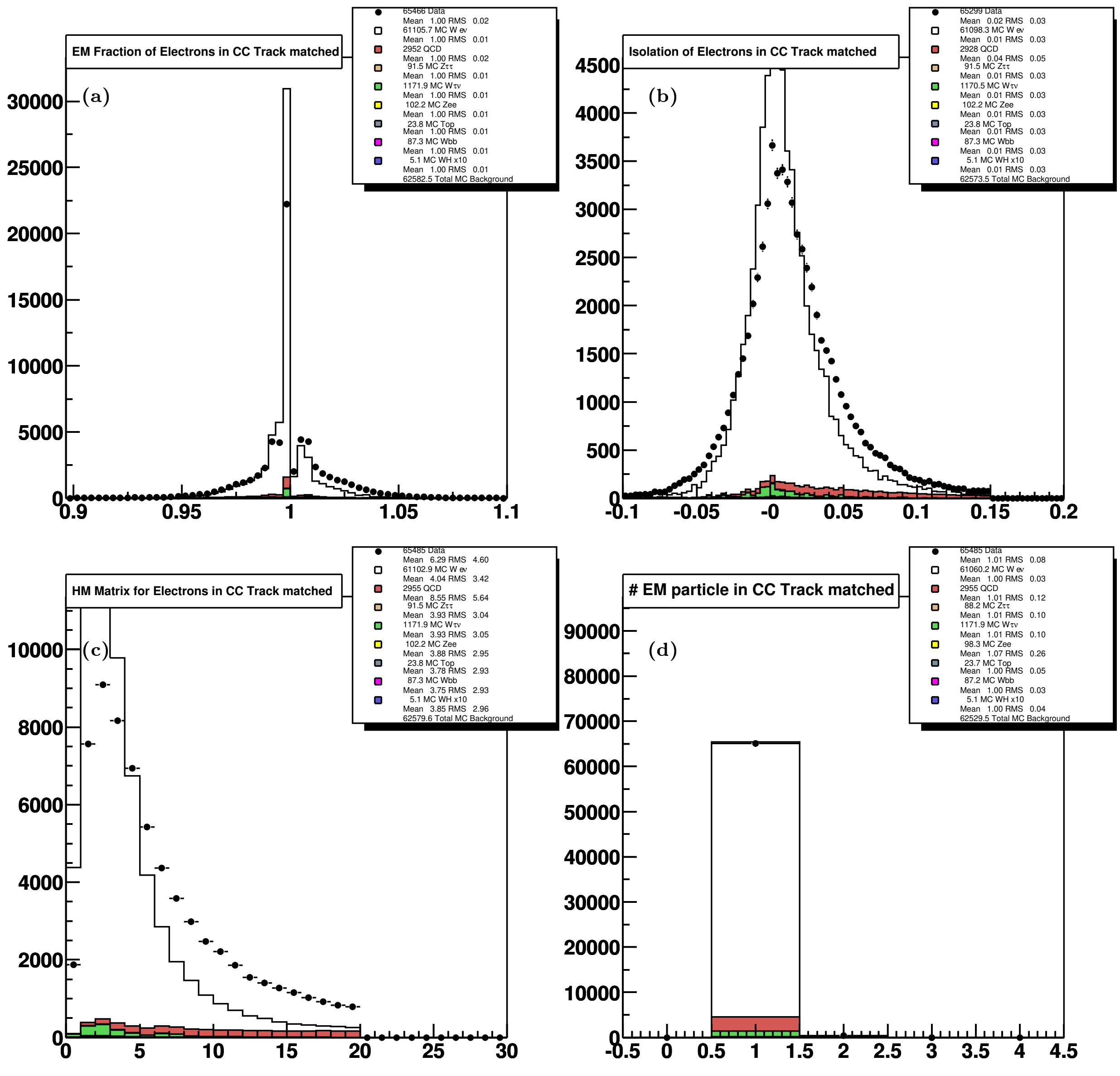

Figure 2: Distributions for electrons with $p_T > 20$ GeV in the final sample. a) E.M. fraction b) isolation; c) H-Matrix. d) multiplicity (the number of events is divided by 100 in the vertical scale);

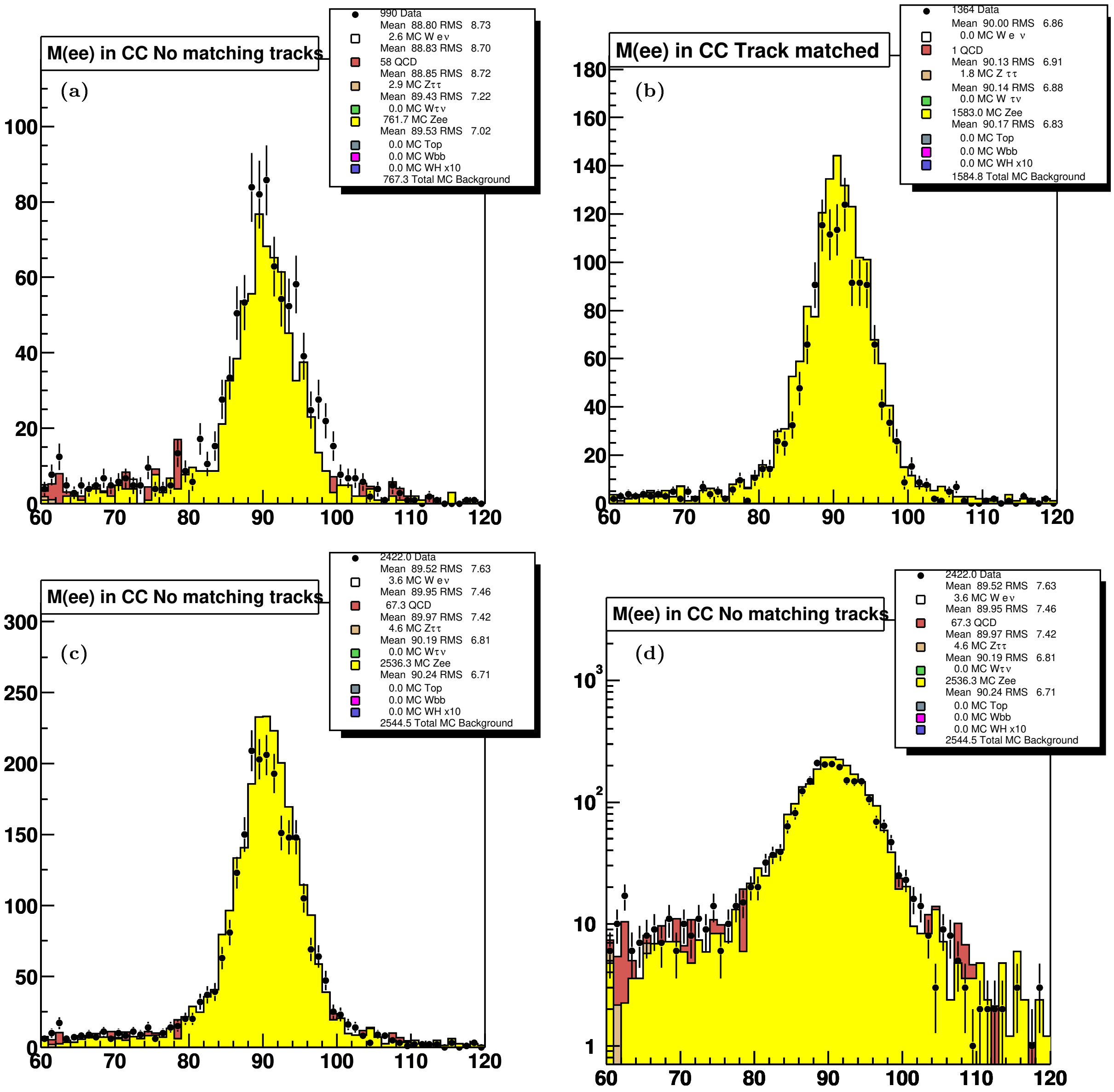

Figure 3: Distributions of the invariant mass of the 2 highest p_T electrons for the final data sample where the missing transverse energy cut has been removed, compared to the simulated expectations, when: a) only one electron has a track match; b) both electrons have a track match; c) at least one electron has a track match (=a+b) d) same as c) in log scale.

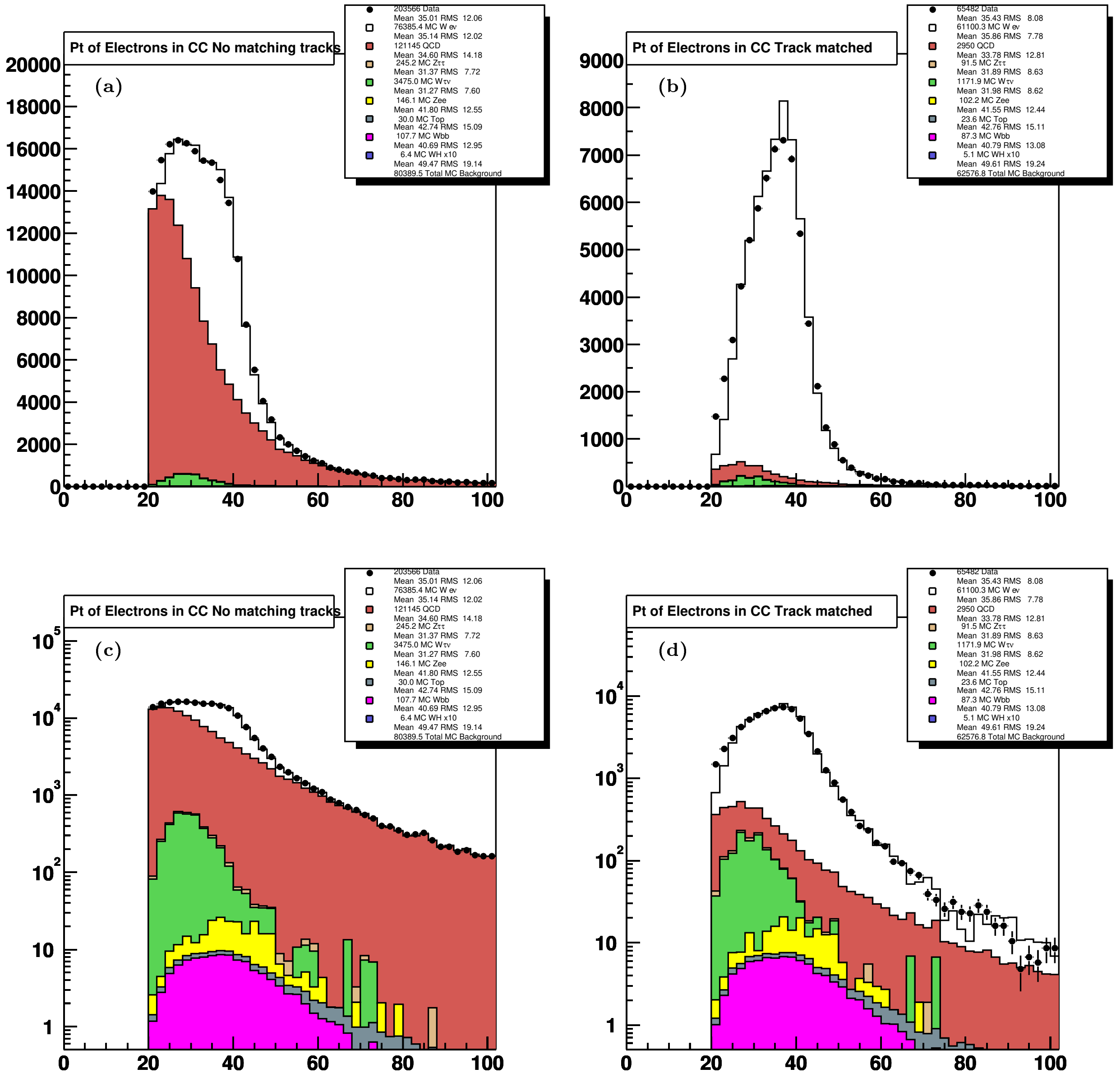

Figure 4: (a) transverse energy of loose electrons (linear scale) (b) transverse energy of tight electrons (linear scale) (c) transverse energy of loose electrons (log scale) (d) transverse energy of tight electrons (log scale)

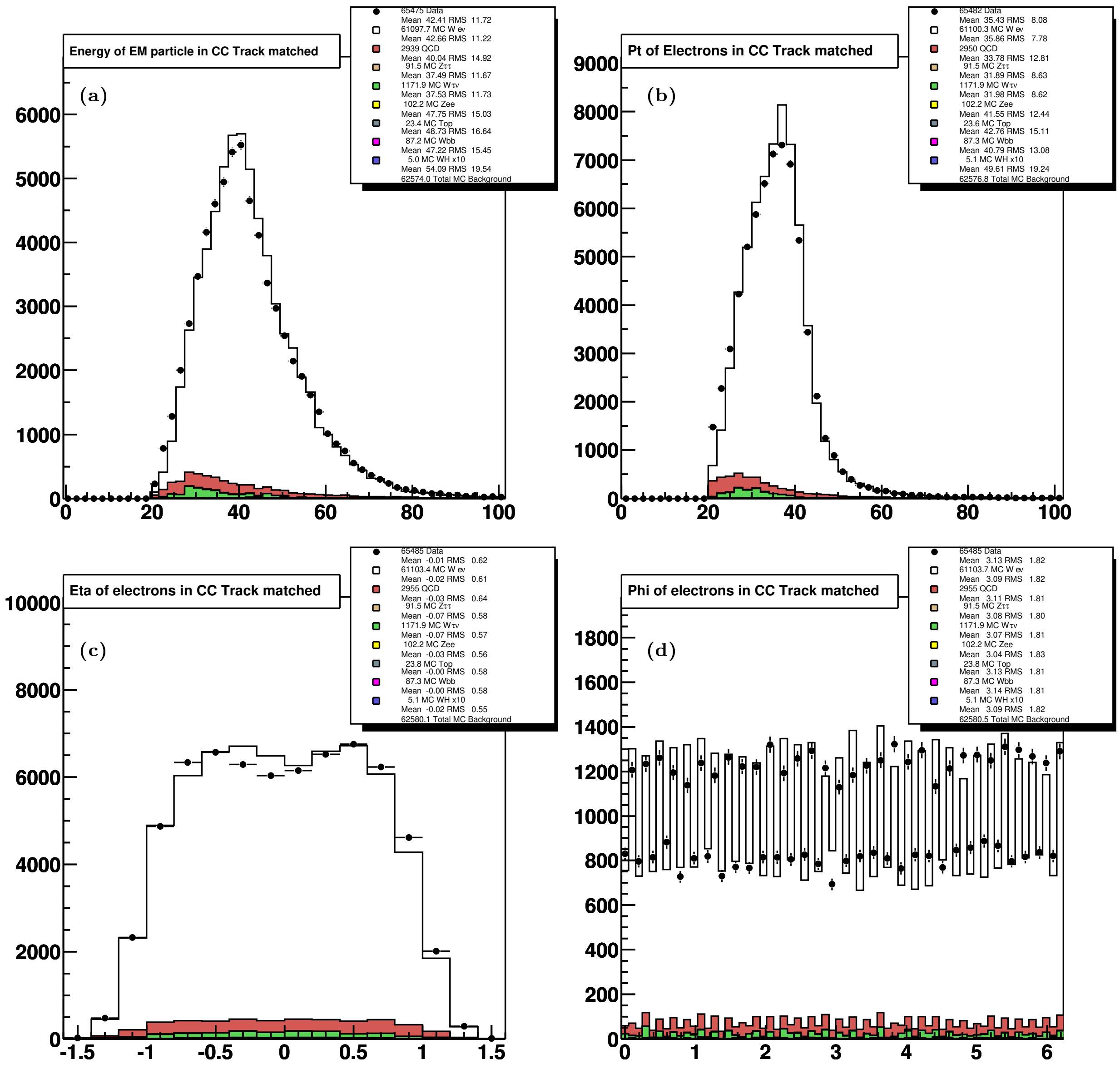

Figure 5: Kinematic distributions for tight electrons in the central calorimeter: a) Energy; b) p_T; c) η; d) φ.

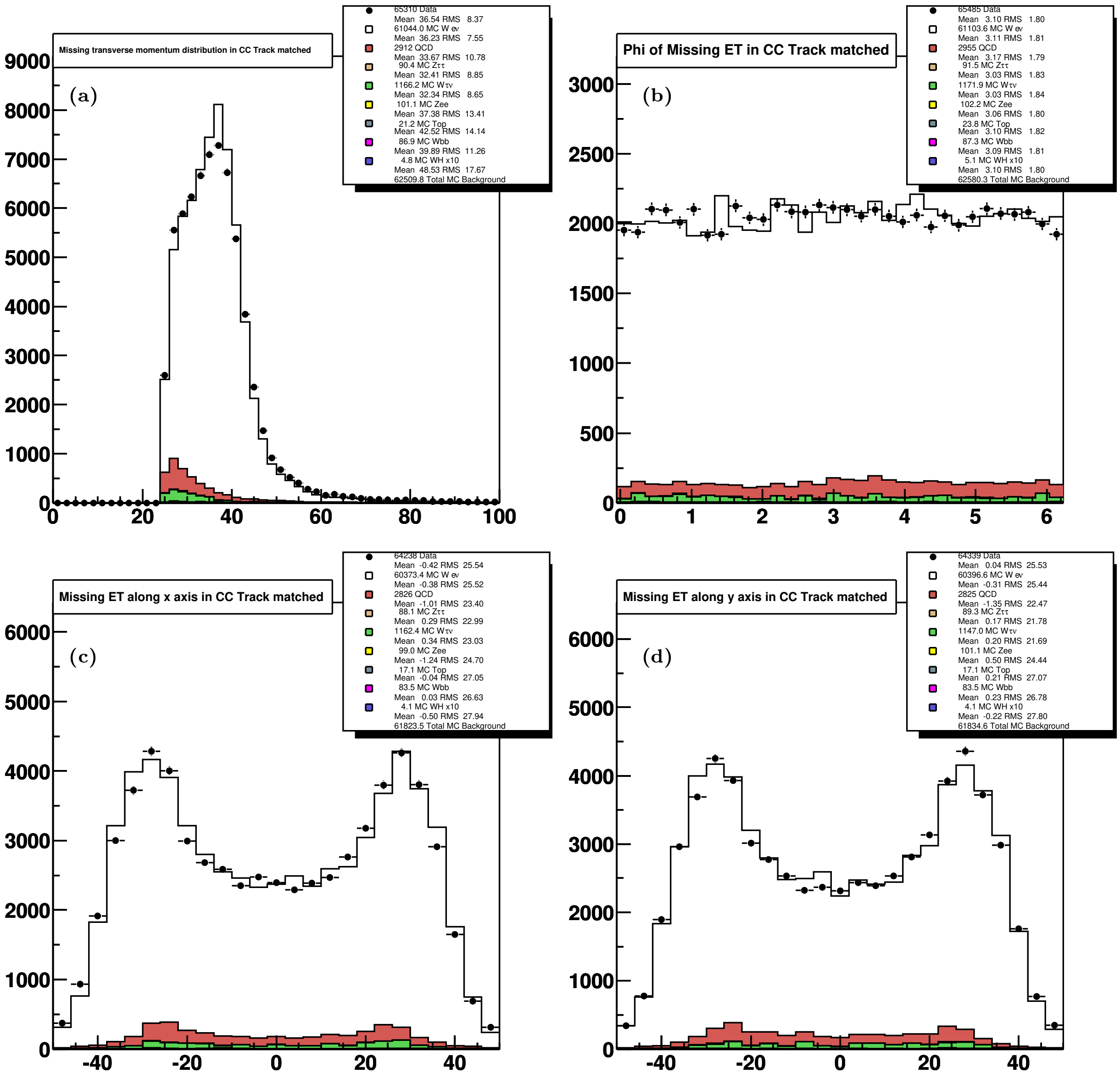

Figure 6: Distributions for missing transverse energy for the final data sample compared to the simulated expectations: a) missing transverse energy; b) azimuthal angle of the missing transverse energy vector; c) $\not\!\!E_T$ along the x axis; d) $\not\!\!E_T$ along the y axis.

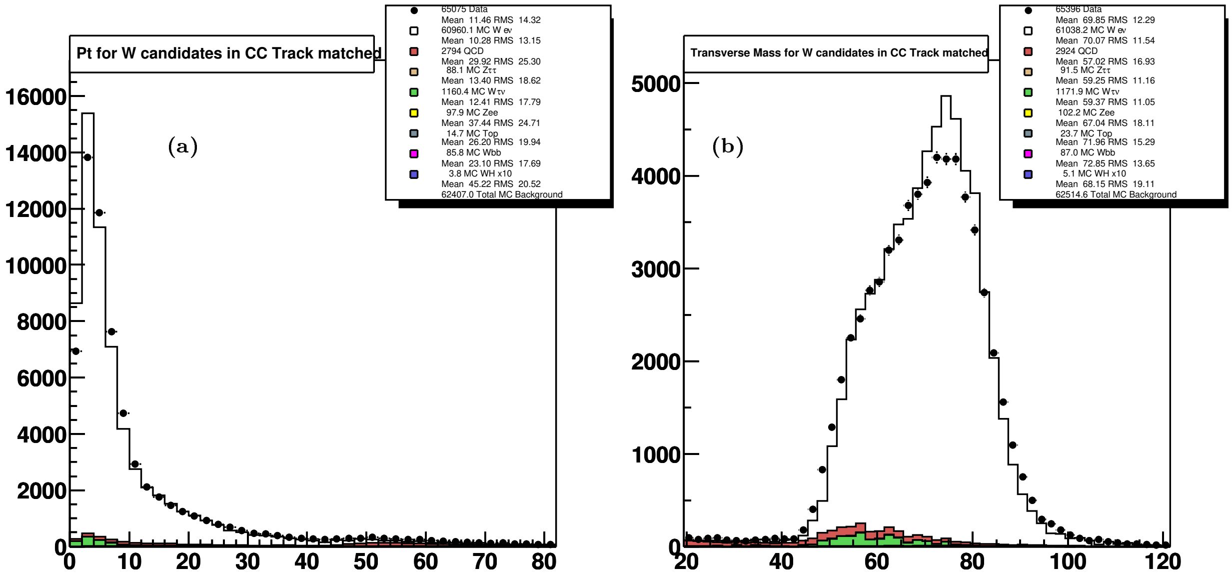

Figure 7: Distributions of the transverse momentum (a) and the invariant mass (b) of the W for the final data sample compared to the simulated expectations.

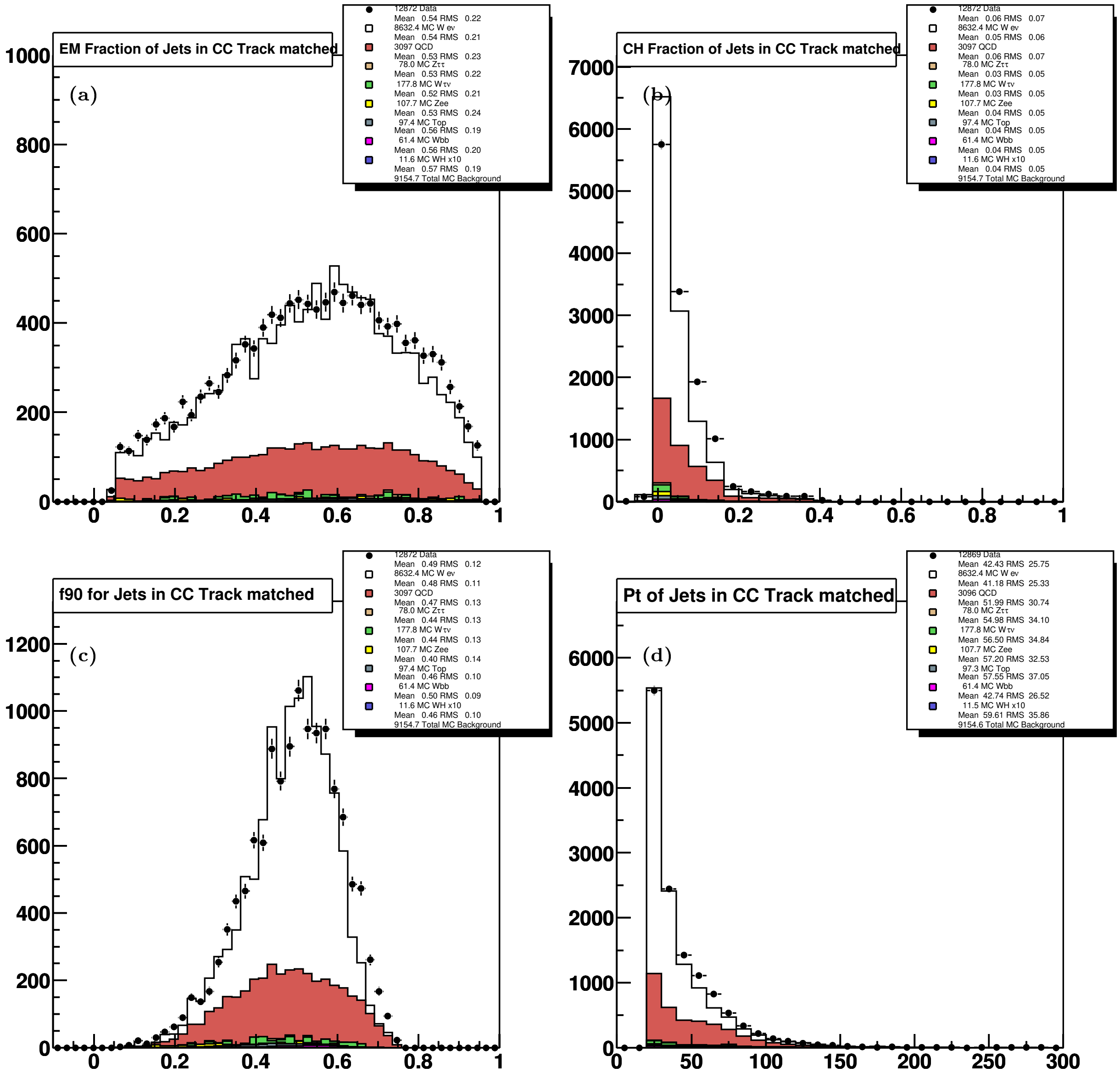

Figure 8: Distributions of the Jet variables of the jets of each event for the final data sample compared to the simulated expectations. a) EM fraction; b) CH fraction; c) f 90; d) P_T. As with all subsequent plot on jets, the simulation is normalized to the data, based on the number of jets in the data substracted from the qcd background. The normalization factor applied to the simulation is 1.21.

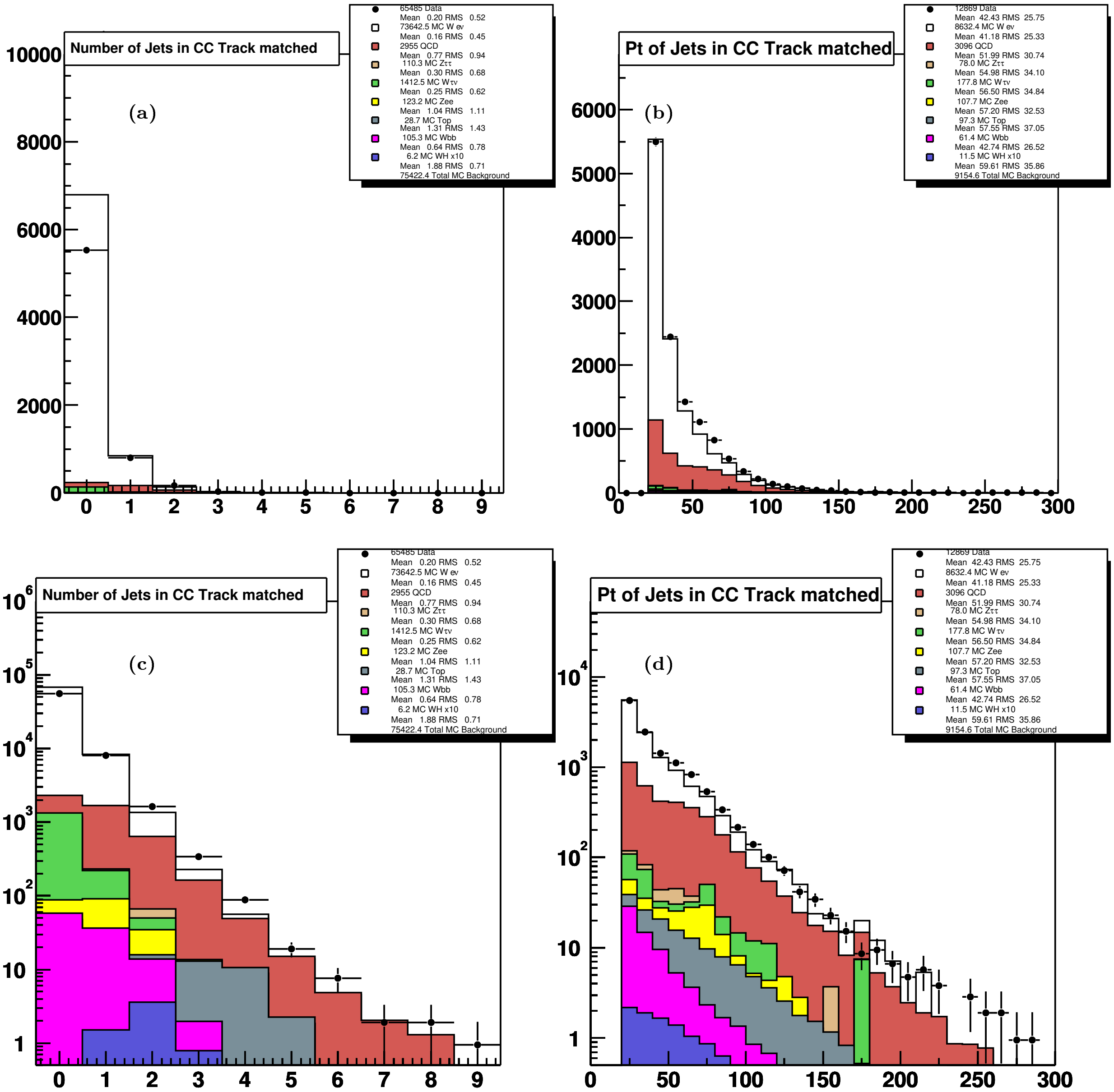

Figure 9: Distributions of the multiplicity and transverse momentum of jets for the final data sample compared to the simulated expectations. a) multiplicity (linear scale) b) transverse momentum of all the jets (linear scale); c) as a) but in log scale; d) as b) but in log scale.

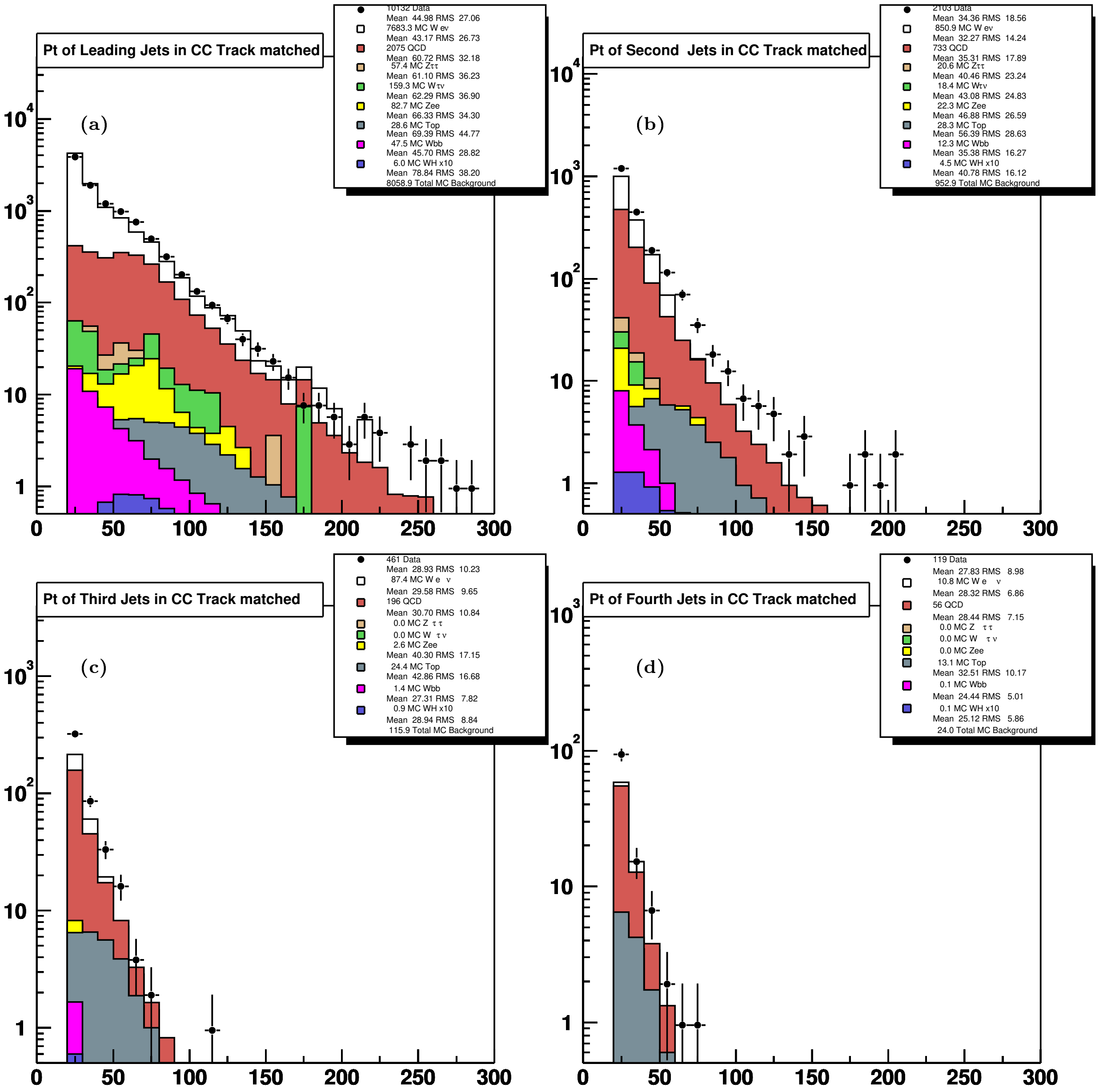

Figure 10: Distributions of the transverse momentum of the jets of each event for the final data sample compared to the simulated expectations. a) leading jet; b) second jet, ordered in p_T; c) third jet; d) fourth jet.

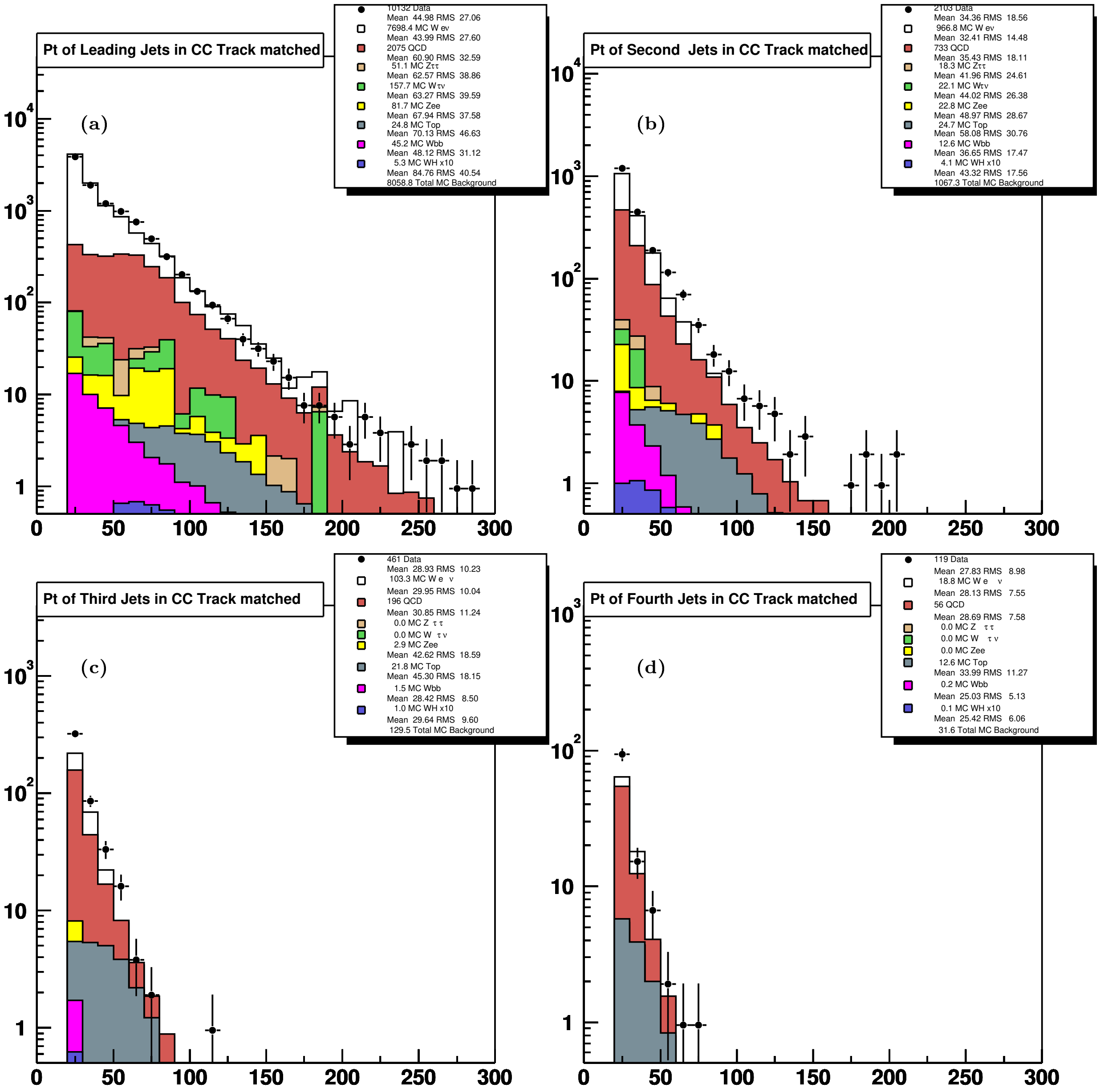

Figure 11: Distributions of the transverse momentum of the jets of each event for the final data sample compared to the simulated expectations, after applying a shift to the jet energy scale (JES) of the simulated jets of one times the uncertainty on the JES, i.e in average +6%. a) leading jet; b) second jet, ordered in p_T; c) third jet; d) fourth jet.

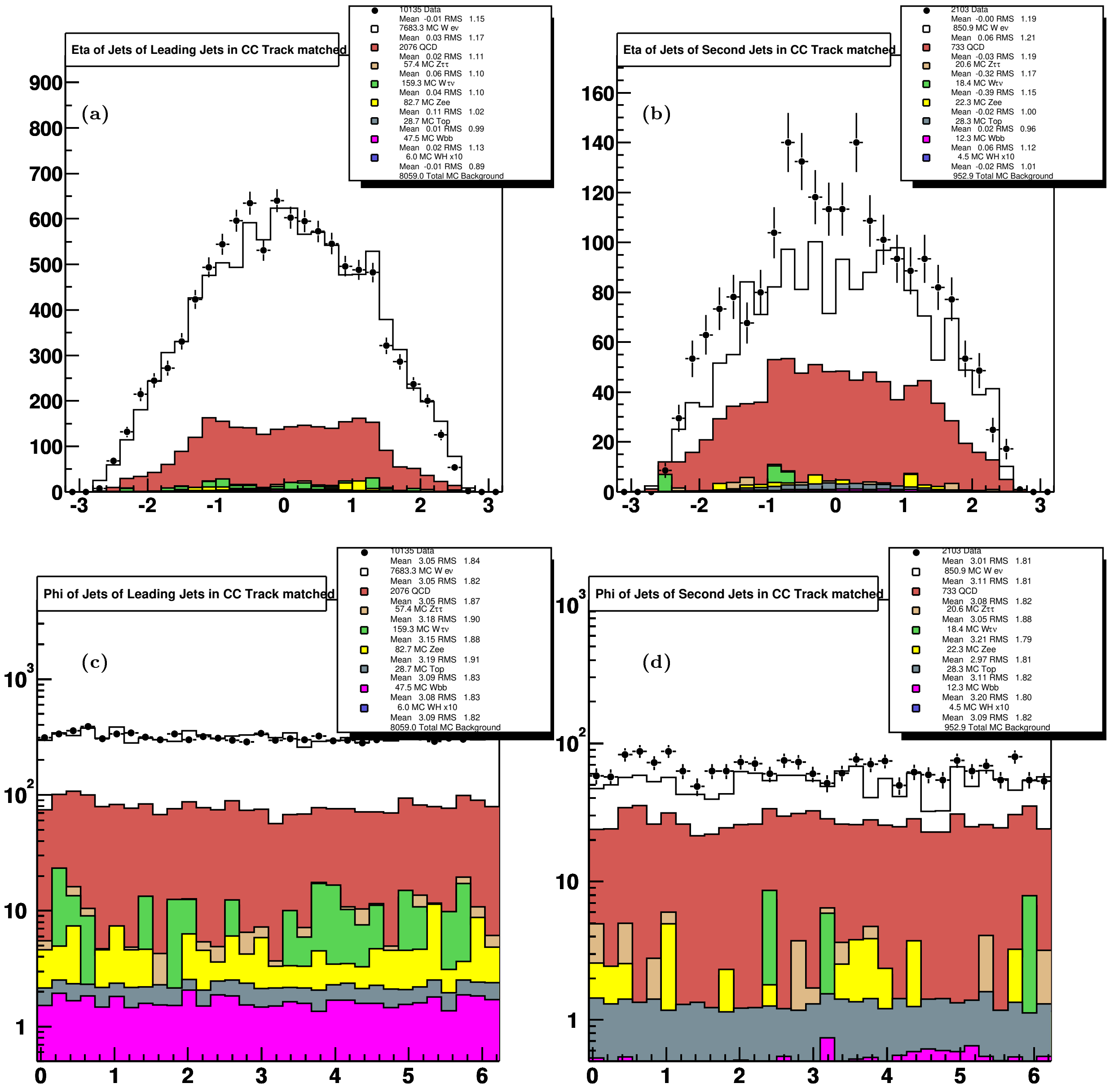

Figure 12: Distributions of η and φ of the two leading jets of each event for the final data sample compared to the simulated expectations: a) η of leading jet; b) φ of leading jet; c) η of second jet; d) φ of second jet;

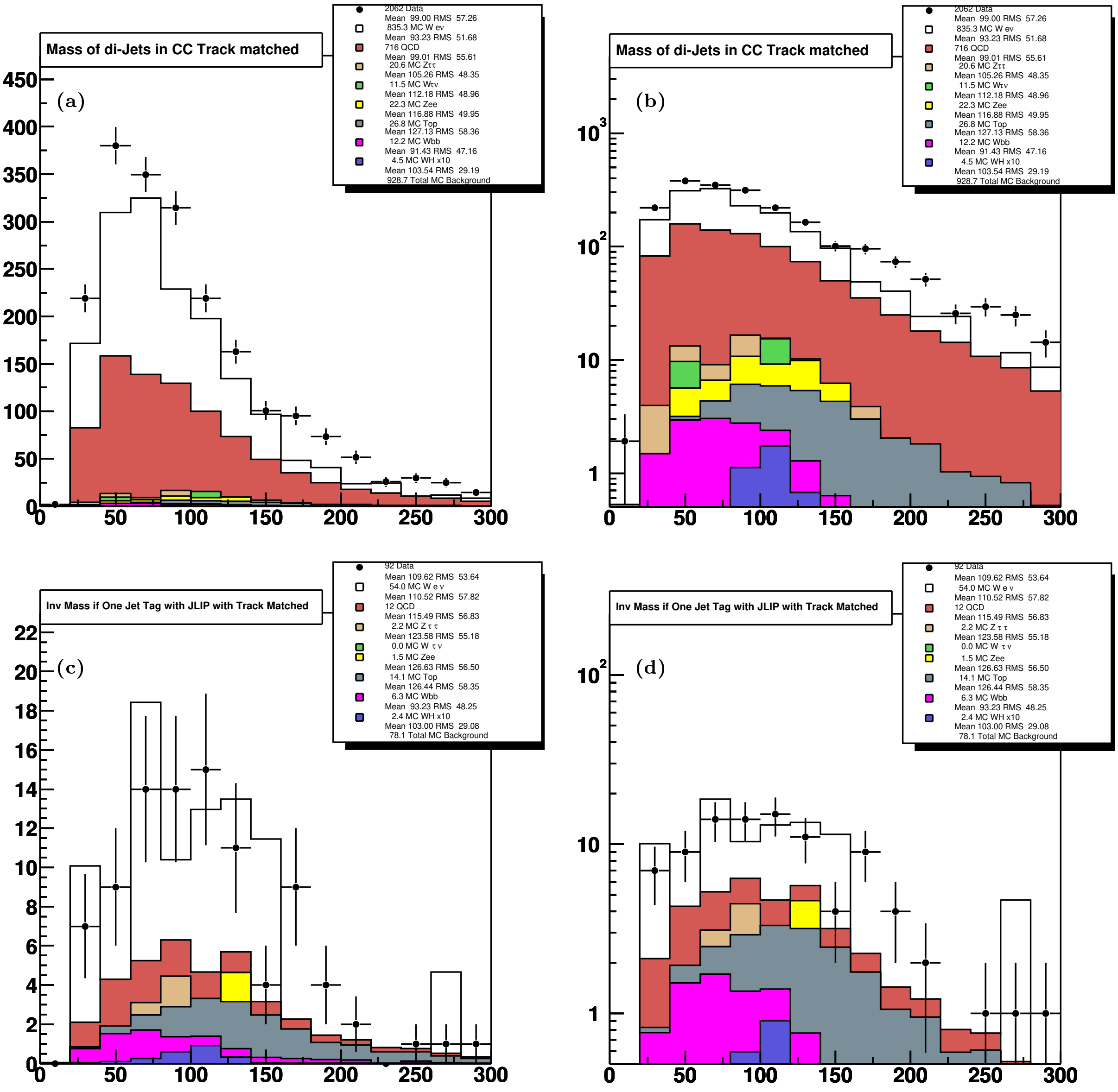

Figure 13: Distribution of the dijet invariant mass, obtained from the two leading jets, for the final data sample compared to the simulated expectations: a) for all events with 2 jets or more; b) same as a) in log scale c) for all events with 2 jets or more, when one jet is b-tagged d) same as c) in log scale.

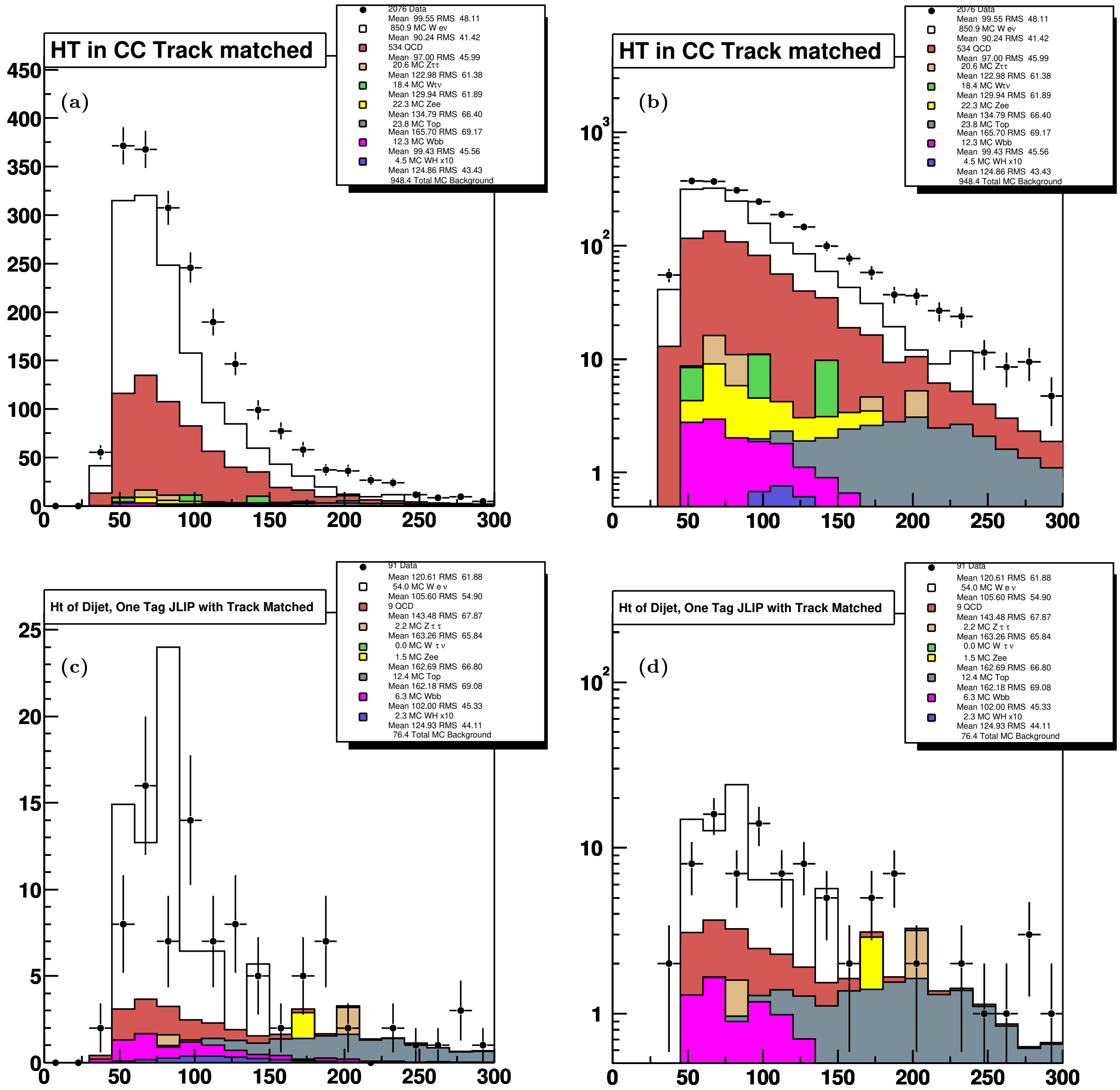

Figure 14: Distribution of the H_T variable ($\equiv$ sum of E_T of all jets) for the final data sample compared to the simulated expectations: a) for all events with 2 jets or more; b) same as a) in log scale c) for all events with 2 jets or more, when one jet is b-tagged d) same as c) in log scale.

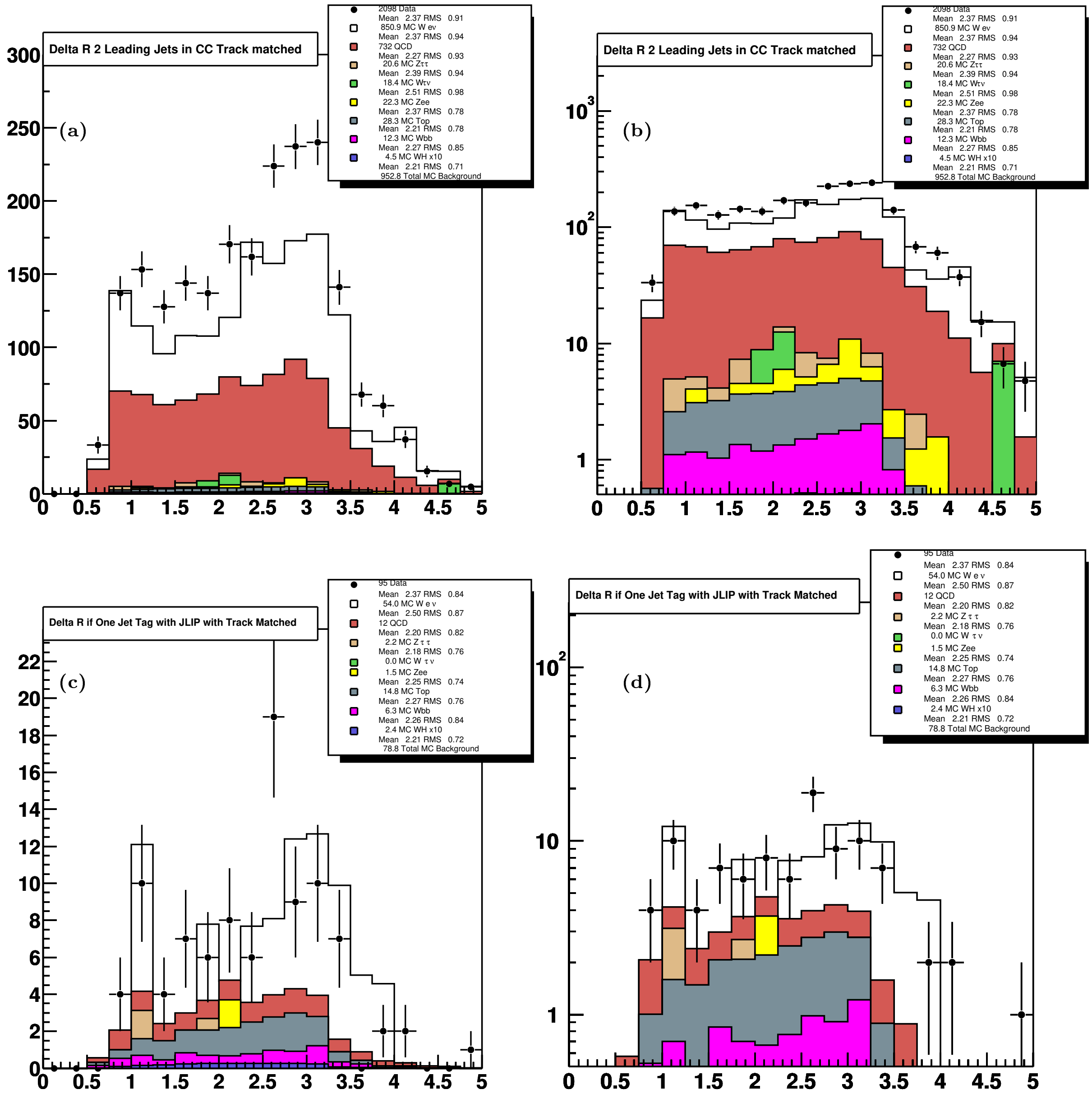

Figure 15: Distribution of ΔR between the two leading jets for the final data sample compared to the simulated expectations: a) for all events with 2 jets or more; b) same as a) in log scale c) for all events with 2 jets or more, when one jet is b-tagged d) same as c) in log scale.

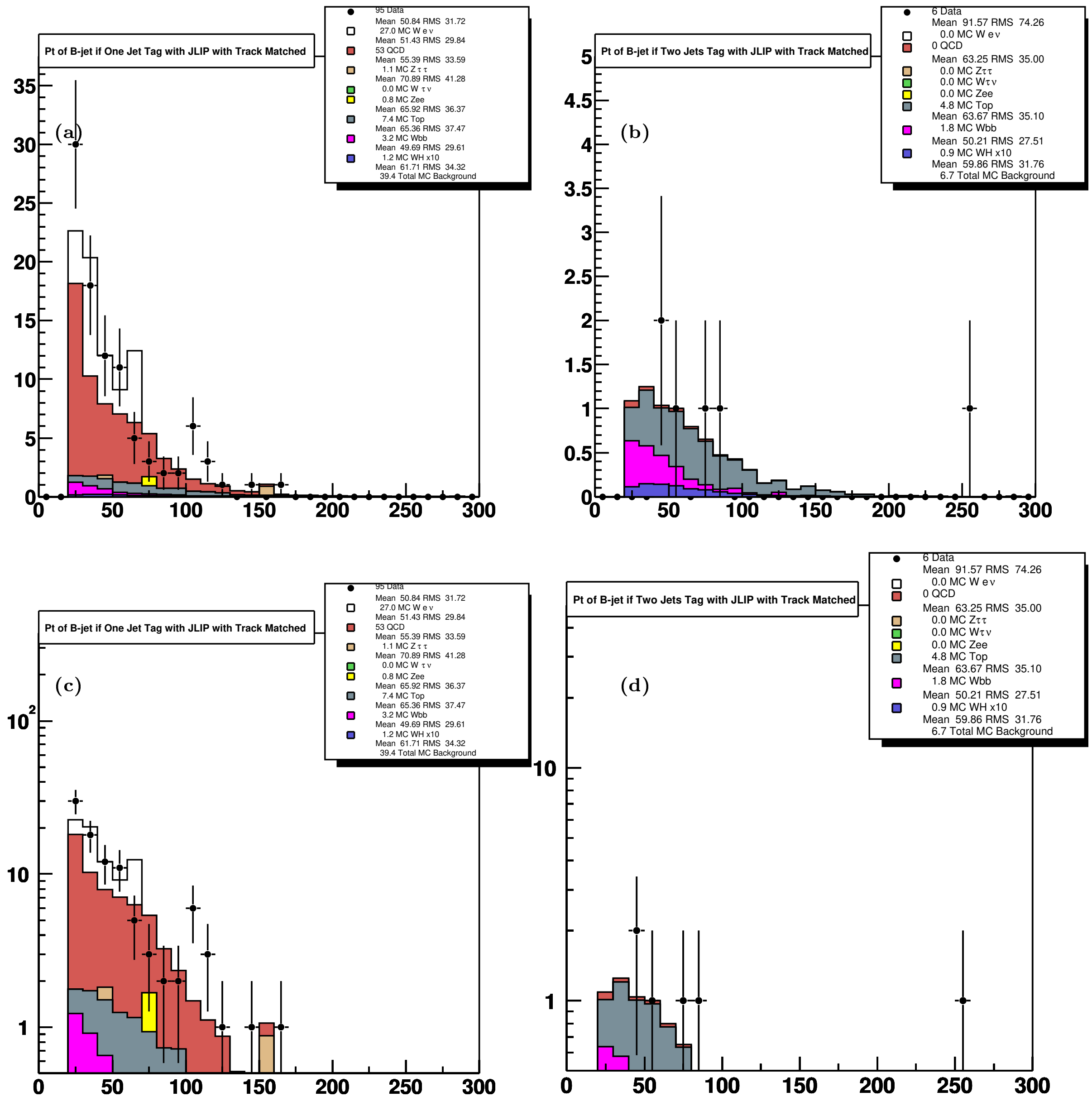

Figure 16: Distributions of the b-tagged jets transverse momentum: a) for the events with 2 or more jets when only one jet is b-tagged b) for the events with 2 or more jets when two or more jets are b-tagged c) same as a) in log scale d) same as b) in log scale

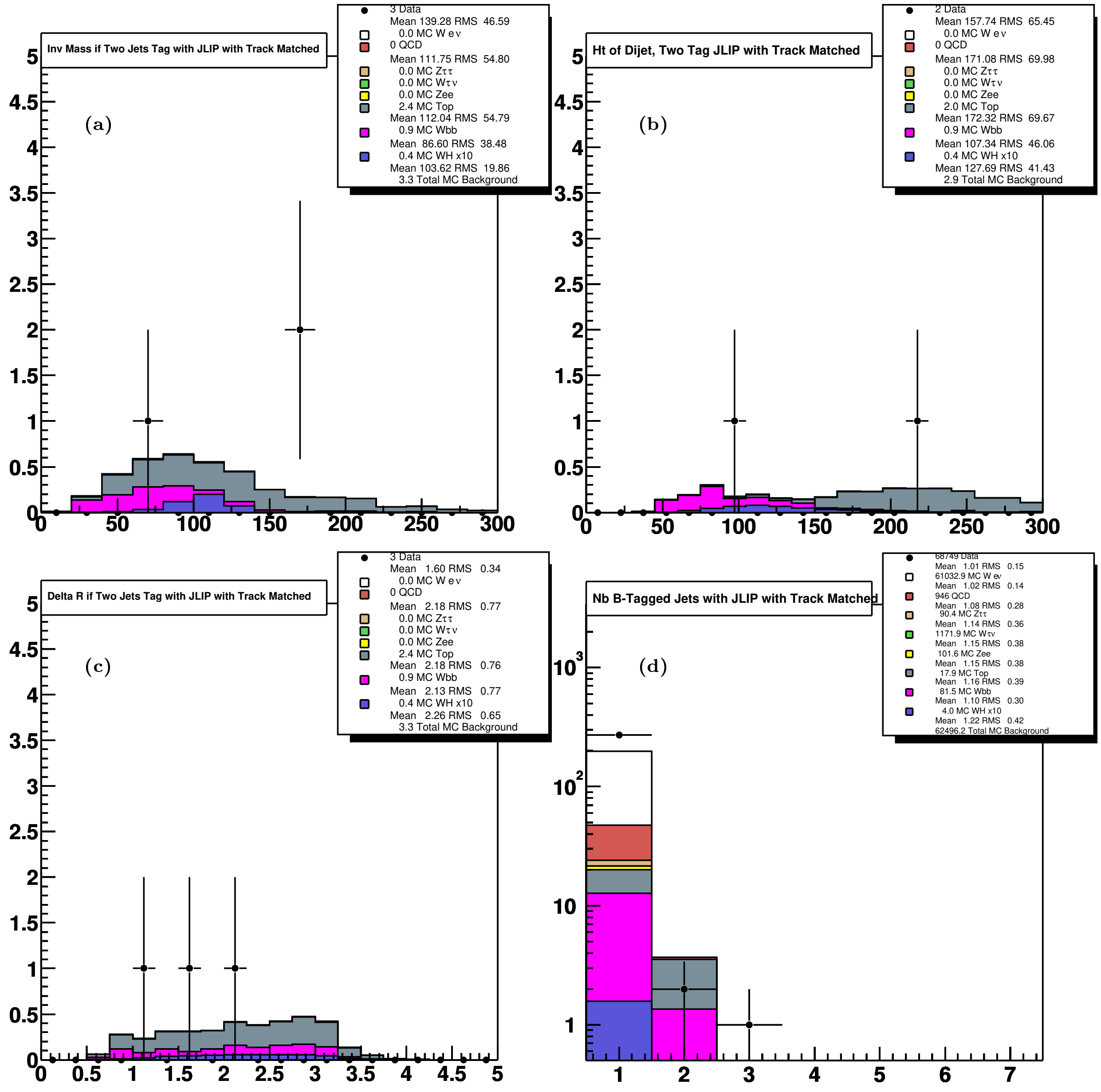

Figure 17: Distributions for the events with 2 or more jets when two or more jets are b-tagged of a) the dijet invariant mass ; b) the H_T variable; c) ΔR between the two leading jets. d) Distribution of the b-tagged jet multiplicity